An AFM study of the genesis and sintering in hydrogen of a realistic Cu/amorphous silica planar model catalyst

Federico J. Williams, Natalie Malikova, and Richard M. Lambert*

Chemistry Department, Cambridge University, Cambridge CB2 1EW, England

Received 15 May 2003; accepted 5 August 2003

The genesis and subsequent sintering in a hydrogen atmosphere of realistic Cu/amorphous silica planar model catalysts have been investigated by atomic force microscopy. Samples were prepared by standard wet chemical methods followed by calcination and reduction, mimicking as closely as possible the procedures used in the preparation of practical, dispersed Cu catalysts. Changes in size distribution and mean particle size are observed as the sequence of transformations, Cu nitrate → cupric oxide → Cu metal, proceeds and an interpretation is offered. Pronounced sintering in hydrogen is the result of migration, agglomeration and coalescence of entire Cu particles, as opposed to Ostwald ripening. A mechanism for this process is proposed on the basis of absorption/desorption of hydrogen at steady state.

KEY WORDS: AFM; Cu/amorphous silica; catalyst genesis, mechanism of; sintering in hydrogen, mechanism of.

1. Introduction

We recently demonstrated the merit of studying the genesis of realistic Ag/single crystal α-alumina model catalysts following wet chemical procedures identical to those used for the synthesis of practical dispersed catalysts [1,2]. It was found that the surface structure of the crystalline alumina support exerted a dramatic influence on the structure and stability of the resulting Ag/α-alumina catalyst. Moreover, these properties were very different from those of nominally identical Ag/α-alumina systems prepared by vacuum deposition of Ag on the same α-alumina surfaces UHV. Studies of such model catalysts under reaction conditions [2] are, therefore, likely to yield fundamental information that is of relevance to an understanding of the behavior of the corresponding practical catalysts that they are intended to mimic.

Here, we have extended this approach to an investigation by atomic force microscopy (AFM) of the genesis and stability of another important and widely studied system Cu/amorphous silica [3–5]. The morphology and stability of nanoscopic Cu particles is important in technical applications, notably methanol synthesis [6–8]. For the same reason, their behavior in hydrogen-containing atmospheres is also of considerable interest [9,10]. Finally, the catalytic properties of silica-supported Cu have played a key role in establishing the mechanism of methanol synthesis [11,12]. We show unambiguously that hydrogen-induced sintering is due to the diffusion, aggregation and coalescence of nanoscopic Cu particles, as opposed to Ostwald ripening.

* To whom correspondence should be addressed.
E-mail: rml1@cam.ac.uk

2. Experimental methods

Copper/amorphous SiO_2/Si(100) model catalysts were prepared by using standard wet chemical methods to deposit Cu particles on an amorphous silica layer produced on a Si(100) surface. Subsequent calcination converted the metal precursor compound to CuO, which was then reduced to yield Cu particles on the silica support. Atomic force microscopy was used to image the sample surface at each stage of this procedure. Particular attention was given to the morphology and size distribution of the Cu nitrate, oxide, and metal particles produced during catalyst genesis. Finally, the sintering behavior in hydrogen was studied.

2.1. Sample preparation

Single crystalline Si(100) wafers (1 × 1 cm) covered with a native oxide layer were cleaned by boiling in a trichlorethylene for 15 min followed by immersion in a 1 : 2 v/v 30% H_2O_2/concentrated H_2SO_4 solution at room temperature for ~30 min. They were then rinsed repeatedly with ultrapure deionized water (resistivity 18.2 MΩ) and dried in flowing nitrogen gas [13,14]. Thereafter, the wafers were kept under vacuum. This treatment is known to produce a uniform capping layer of amorphous silica [14]. XPS examination showed that in our case the procedure resulted in clean silica surfaces ~2.5 nm thick on top of the underlying Si(100) surface. (The thickness was estimated from the attenuation by

1011-372X/03/1000–0177/0

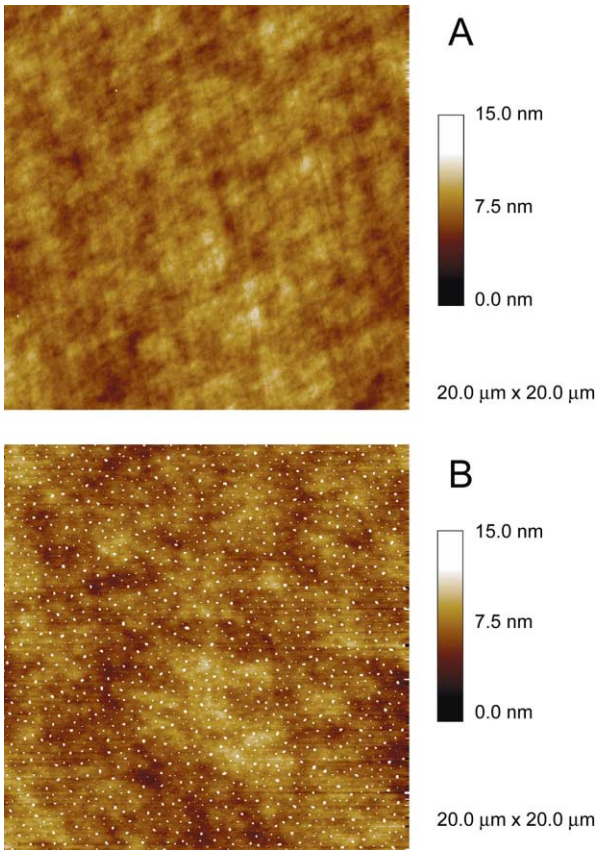

Figure 1. AFM images of (A) clean amorphous silica surface and (B) silica surface after Cu nitrate deposition.

the silica-capping layer of the Si^0 2p emission from the Si(100) substrate). An atomizer (Agar Scientific) was used for uniform spray deposition of $\sim 80\,\mu L$ of a $9.3 \times 10^{-3}\,mol^{-1}\,dm^{-3}$ Cu nitrate solution onto the silica surface at room temperature.

2.2. Sample treatment

The Cu nitrate-deposited wafers were sequentially subjected to three treatments, namely (i) calcination; (ii) reduction in hydrogen; and (iii) sintering in hydrogen. Calcination was performed under a continuous flow of 20% O_2 in He (40 cm^3/min) while raising the temperature (2 K/min) from 300 K to 573 K; the samples were then held at 573 K for 4 h before cooling to room temperature. Reduction was carried out in flowing 15% H_2 in He (40 cm^3/min), ramping the temperature (2 K/min) from room temperature to 503 K, maintaining 503 K for 4 h and then cooling to room temperature. Finally, the samples were sintered at 673 K for 8 h in 15% H_2 in helium (40 cm^3/min). XPS analysis showed that the reduction step caused the conversion of the Cu oxide particles to metallic Cu without any accompanying change in the oxidation state of silica support. This chemical composition remained unaltered by the subsequent high-temperature sintering stage.

2.2.1. AFM characterization

Imaging was performed under ambient conditions in tapping mode (Dimension Digital Instruments D 3100 - Nanoscope IV). The probes were silicon cantilevers (MikroMasch Eesti Ltd., NSC15 resonant frequency 330–370 kHz, force constant ~ 40 N/m) with integrated silicon tips (tip height 15–20 μm, maximum tip curvature 10 nm). The AFM tips were checked regularly by imaging HOPG graphite to ensure sharpness of the tip and to verify the absence of tip artefacts. The samples were immobilized on the microscope stage by vacuum suction. This allowed convenient, non-destructive specimen removal, thus enabling the same sample to be examined and re-examined at each of the stages outlined above. All the images presented here are representative in that essentially the same features were observed all over the (very large) accessible sample area (10× 10 mm).

3. Results and discussion

Figure 1(A) shows an image of the clean amorphous silica surface. No foreign deposits were observed in large-area scans ($20 \times 20\,\mu m^2$), and the surface showed a roughness amplitude of 4 nm, peak-to-peak. XPS measurements showed no detectable surface impurities. The thickness of the amorphous silica layer remained unchanged throughout the calcinations, reduction and sintering steps. Figure 1(B) shows a typical image obtained after the Cu nitrate deposition from aqueous solution. The homogeneity of the deposited salt on a scale of $20 \times 20\,\mu m$ is striking and illustrates the effectiveness of our simple atomizer spray procedure.

The left panel of figure 2(A) ($3 \times 3\,\mu m^2$) shows the Cu nitrate deposit in greater detail. The corresponding particle size distribution is shown in the right panel of figure 2(A). This bimodal distribution is dominated by (i) single particles, approximately hemispherical, of $\sim$60–nm mean diameter and (ii) agglomerates of such particles of $\sim$125–nm mean diameter. Since the surface-cleaning procedure used prior to Cu nitrate deposition yields a fully hydroxylated silica surface (OH surface density 5.0 nm^{-2}) [15], it seems unlikely that the bimodal distribution is due to crystallite nucleation and growth [16] on a patchily hydroxylated surface. It may be an artefact of the spray-deposition technique; for our purposes, the key point is the homogeneity of the deposit and the relatively narrow overall particle-size distribution.

Figure 2(B) (left panel) shows an AFM image taken after calcination of the nitrate deposit shown in figure 2(A). Note that nitrate $\rightarrow$ oxide conversion results in (i) a higher particle density (increased by a factor of

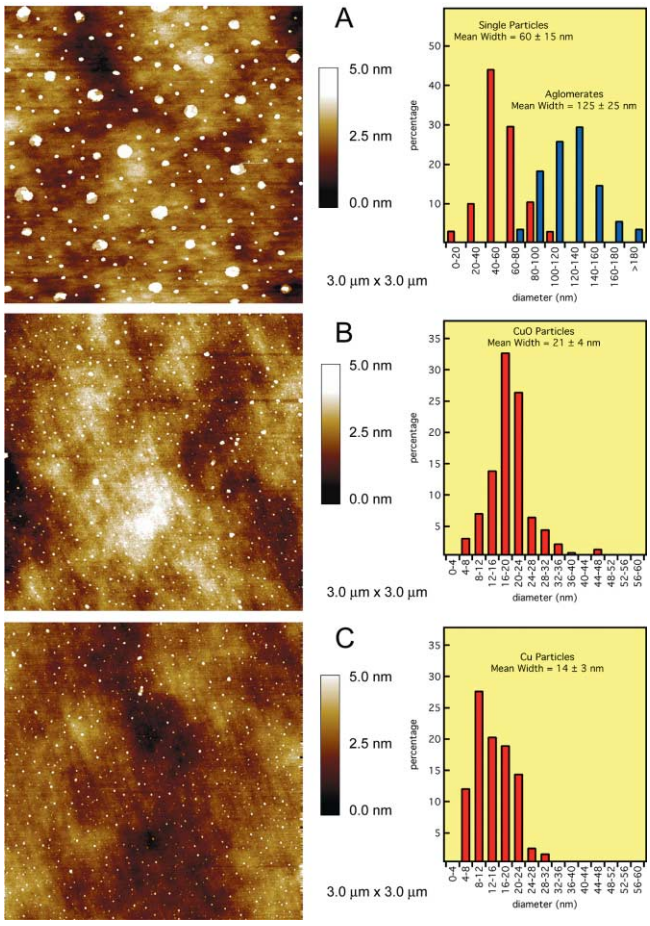

Figure 2. AFM images (left panel) and particle-size distributions (right panel) after (A) Cu nitrate deposition, (B) calcination, and (C) reduction in hydrogen.

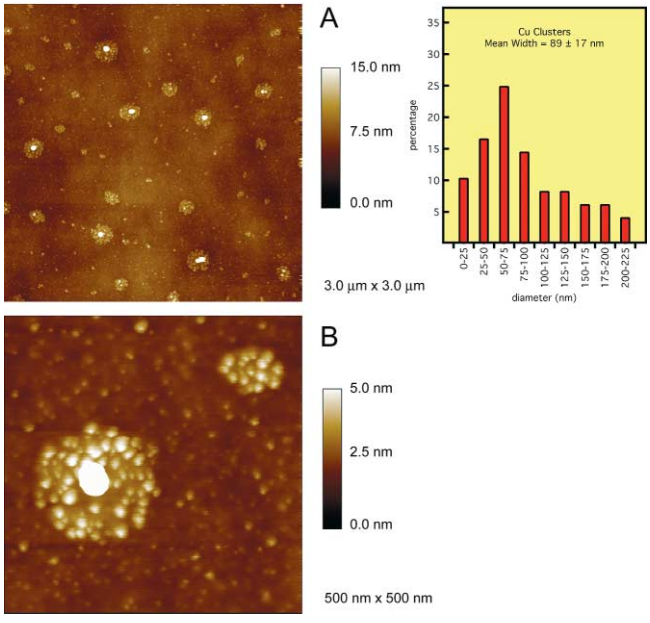

Figure 3. (A) AFM image (left panel) and particle-size distribution (right panel) of the silicon sample after sintering in hydrogen at 673 K for 8 h. (B) Detailed view of an agglomerated Cu cluster.

~3.7) and (ii) replacement of the bimodal size distribution by a normal distribution. This is illustrated in the right panel of figure 2(B), which shows that the particle-size distribution of the Cu oxide particles corresponds to ~21 nm of mean diameter. Note that the Cu nitrate particles are likely to have been hydrated, which would be consistent with the large size decrease that accompanied conversion to the oxide.

Figure 2(C) (left and right) show, respectively, AFM images obtained after hydrogen reduction of the CuO particles shown in figure 2(B) and the corresponding particle-size distribution. Reduction to the metallic state did not cause significant morphological changes, and the particle density was essentially unchanged. The mean particle Cu diameter is 14 nm, which is in good accord with the calculated 43% volume decrease expected when the oxide is converted to the metal.

The sintering behavior of the Cu/silica system in hydrogen (673 K/8 h) is made strikingly apparent by the AFM results shown in figure 3(A) (left). It is evident that a dramatic change in morphology occurred—this "snapshot", which refers to a particular sintering time and temperature, shows that the initially uniform distribution of Cu has been replaced by structures in which agglomeration of small Cu particles around larger Cu cores has occurred. The particle-size distribution is shown in the right panel of figure 3(A). The mean diameter of these agglomerates was ~90 nm, compared to the 14-nm mean diameter of the initial Cu particles shown in figure 2(C). Furthermore, the size of the central core is greater than that of the initial (unsintered) Cu particles, implying that the core results from fusion of these initial Cu particles. Presumably, at sufficiently long times or high temperatures, this coalescence process would go to completion. Indeed, although figure 3(A) is representative of the state of the sample, we did occasionally observe large fully coalesced Cu particles without the surrounding halo of small particles. An agglomerated Cu cluster is shown in more detail in figure 3(B).

Finally, we note that representative particle densities for the different cases were as follows: 24.7 μm^{-2} (Cu nitrate, figure 2(A)), 91.4 μm^{-2} (Cu oxide, figure 2(B)), 94.2 μm^{-2} (unsintered Cu metal, figure 2(C)) and 56.1 μm^{-2} (agglomerates, figure 3(A)). These values follow the expected trend and confirm that figure 3 corresponds to a lower density of coalescing particles than the density of unsintered Cu particles in figure 2(C).

The sintering behavior of dispersed metal catalysts is often critically important in determining whether a given material is likely to be of practical use in the long term. Accordingly, sintering mechanisms are of considerable interest. However, these mechanisms are notoriously difficult to establish in any given case. Although discussions normally focus on two possibilities, Ostwald ripening (which depends on atomic

diffusion) versus migration of entire nanoscopic particles—although it is very rare that firm conclusions are reached.

Here, the experimental evidence suggests the following: sintering of Cu particles on amorphous silica occurs by migration, agglomeration, and coalescence of nanoscopic metal particles and *not* by Ostwald ripening. Interestingly, in the case of Ag on crystalline α-alumina [1], our results pointed to Ostwald ripening as the sintering mechanism. To our knowledge, the only other comparable demonstration of sintering by nanoparticle migration is provided by the work of Goodman *et al*. for Au on TiO_2 [17]. Why does hydrogen have this effect? A clue is provided by the results of Elliott *et al*. who found that under conditions similar to ours, nanoscopic Cu particles absorb large amounts of hydrogen [10]. At steady state, continuous absorption/desorption of hydrogen at the Cu/silica interface could weaken the interaction between the two phases, thus permitting diffusion of entire Cu particles.

4. Conclusions

1. Realistic Cu/amorphous silica planar model catalysts suitable for investigation by scanned probe microscopy may be prepared by application of standard wet chemical methods followed by calcination and reduction.

2. Observed changes in mean particle size and size distribution of the Cu-containing crystallites are quantitatively consistent with the sequence of transformations, Cu nitrate $\rightarrow$ cupric oxide $\rightarrow$ Cu metal.

3. Sintering in hydrogen is the result of migration, agglomeration and coalescence of entire Cu particles.

Acknowledgments

F.J.W. acknowledges the award of a Cambridge University Oppenheimer Research Fellowship. We are grateful for the invaluable assistance of Dina Rosh during the AFM experiments.

References

[1] D.P.C. Bird, C.M.C. de Castilho and R.M. Lambert, Surf. Sci. 449 (2000) L221.
[2] S. Wodiunig, J.M. Keel, T.S.E. Wilson, F.W. Zemichael and R.M. Lambert, Catal. Lett. 87 (2003) 1.
[3] X. Xu, S.M. Vesecky and D.W. Goodman, Science 258 (1992) 788.
[4] X. Xu, S.M. Vesecky, J.W. He and D.W. Goodman, J. Vac. Sci. Technol., A 11 (1993) 1930.
[5] R. van Wijk, O.L.J. Gijzeman, J.W. Geus, E. ten Grotenhuis and J.C. van Miltenburg, Catal. Lett. 24 (1994) 171.
[6] R.A. Hadden, B. Sakakini, J. Tabatabbei and K.C. Waugh, Catal. Lett. 44 (1997) 145.
[7] K.C. Waugh, Catal. Lett. 58 (1999) 163.
[8] A.J. Elliott, M.J. Watson, J. Tabatabei, F.W. Zemichael and K.C. Waugh, Catal. Lett. 79 (2002) 1.
[9] G.J. Millar, C.H. Rochester and K.C. Waugh, Catal. Lett. 14 (1992) 289.
[10] A.J. Elliott, B. Sakakini, J. Tabatabei, K.C. Waugh, F.W. Zemichael and R.A. Hadden, J. Chem. Soc. Faraday Trans. 91 (1995) 3659.
[11] G.C. Chinchen, K.C. Waugh and D.A. Whan, Appl. Catal. 25 (1986) 101.
[12] G.C. Chinchen, M.S. Spencer, K.C. Waugh and D.A. Whan, Appl. Catal. 32 (1987) 371.
[13] A. Ishizaka and Y. Shiraki, J. Electrochem. Soc. 133 (1986) 666.
[14] W. Kern, J. Electrochem. Soc. 137 (1990) 1887.
[15] A. Ulman, *An Introduction to Ultra-thin Organic Films: From Langmuir–Blodgett to Self-assembly* (Academic Press, Boston, MA, 1991).
[16] E. ten Grotenhuis, J.C. van Miltenburg, J.P. van der Eerden, R. van Wijk, O.L.J. Gijzeman, J.W. Geus and C.H.M. Maree, Catal. Lett. 28 (1994) 109.
[17] A. Kolmakov and D.W. Goodman, Rev. Sci. Instrum. 74 (2003) 2444.